Enhanced Stability and Controlled Delivery of MOF-Encapsulated Vaccines and Their Immunogenic Response In Vivo

Michael A. Luzuriaga,[†,§] Raymond P. Welch,[†,§] Madushani Dharmarwardana,[†] Candace E. Benjamin,[†] Shaobo Li,[†] Arezoo Shahrivarkevishahi,[†] Sarah Popal,[†] Lana H. Tuong,[†] Chayton T. Creswell,[†] and Jeremiah J. Gassensmith*[,†,‡]

[†]Department of Chemistry and Biochemistry, and [‡]Department of Biomedical Engineering, The University of Texas at Dallas, 800 West Campbell Road, Richardson, Texas 75080, United States

Ⓢ *Supporting Information*

ABSTRACT: Vaccines have an innate tendency to lose their structural conformation upon environmental and chemical stressors. A loss in conformation reduces the therapeutic ability to prevent the spread of a pathogen. Herein, we report an in-depth study of zeolitic imidazolate framework-8 and its ability to provide protection for a model viral vector against denaturing conditions. The immunoassay and spectroscopy analysis together demonstrate enhanced thermal and chemical stability to the conformational structure of the encapsulated viral nanoparticle. The long-term biological activity of this virus-ZIF composite was investigated in animal models to further elucidate the integrity of the encapsulated virus, the biosafety, and immunogenicity of the overall composite. Additionally, histological analysis found no observable tissue damage in the skin or vital organs in mice, following multiple subcutaneous administrations. This study shows that ZIF-based protein composites are strong candidates for improved preservation of proteinaceous drugs, are biocompatible, and are capable of controlling the release and adsorption of drugs in vivo.

KEYWORDS: *vaccine, MOF, ZIF-8, metal−organic frameworks, biomimetic mineralization, virus-like particles*

Proteinaceous therapeutics are moving to the forefront of medicine for their specificity in treatments, favorable side effect profiles, and their potential in personalized medicine.[1,2] Unfortunately, many of these proteins are structurally metastable[3] and they can undergo drastic conformational changes at elevated temperatures, in organic solvents, and at pHs different from physiological conditions.[4,5] These problems limit proteins to short-term low-temperature storage that require costly infrastructure in place to keep them stable throughout shipping. Researchers have been motivated by these limitations and have begun to develop new methods that can enhance protein stability.[6−12]

Metal−organic framework (MOF) encapsulation has been shown[13] to stabilize enzymes,[14,15] viruses,[16,17] and antibodies[18] while providing structural and chemical protection. MOFs are highly porous crystalline materials made of metal-ion clusters linked by organic ligand struts[19,20] that have shown promise for use in gas storage[21] and separation,[22,23] catalysis,[24,25] sensing,[26] and small molecule drug delivery.[27−30] Recently, researchers have shown that MOFs can immobilize[31,32] and stabilize[33,34] biomacromolecules. In particular, coating proteins in zeolitic imidazolate framework-8 (ZIF-8) is proving to be a promising method for protection against conditions normally adverse to proteins, and there have been many promising advancements in this area.[33,35−38] In particular, biomimetic mineralized growth[15,16,32] of ZIF-8 directly onto the surface of a protein has emerged as a means to encapsulate enzymes and insulin using only protein, zinc salts, and methylimidazole directly in water.[39,40] Because ZIF-8 can grow on protein surfaces of different sizes, charge states, and morphologies, this process is quite "agnostic" to the biomolecule host inside the ZIF.[17,36] This differs from other equally elegant methods that use bespoke MOFs with tuned[41−43] pore sizes to encapsulate specific biomolecules or polymer-encapsulated proteins coated with ZIF and formed in organic protic solvents.[44,45] For instance, our lab biomimetically encapsulated tobacco mosaic virus (TMV) within a ZIF-8 shell (TMV@ZIF) and found the encapsulation process to be high yielding and promoted by a modest affinity for zinc ions toward the proteinaceous surface.[17] This affinity leads to high local concentrations of zinc, which promotes a mineralization process that results in either core−shell or monolithic crystals of bionanoparticles.[15,46] It is unclear, however, how—or if—the nucleation and growth affects the secondary or tertiary structure at the protein surface. If the protein surface of a therapeutic protein is

altered as a result of the nucleation process, unwanted immunological reactions may occur as human proteins would not be recognized as "self" and antigens for encapsulated vaccines would raise antibodies against a misfolded protein rendering this strategy moot.[47−49] Because an articulated aim[32] of thermally stabilizing proteins is to improve the global distribution of vaccines, which depend upon the fidelity of their folded structure, we were drawn to determine if changes in the immunogenicity of a viral nanoparticle would emerge following encapsulation and administration.

We chose TMV, a 300 nm × 18 nm tubular RNA plant virus, as a model vaccine biomacromolecule owing to extensive data on its in vivo performance as a carrier for engineered and chemically conjugated[50−52] epitopes in vaccine development (Scheme 1). This chemical modifiability, which can occur on

Scheme 1. Schematic for Analyzing Surface Effects from Encapsulation and Stressing: TMV Contains Glutamate Residues, Shown in Blue, on the Interior Pore Modifiable with EDC Chemistry; The Viral RNA, Shown in Orange, is Embedded Inside the TMV Pore; (a) Native TMV is Incubated with 2-Methylimidazole and Zinc Acetate to form TMV@ZIF; (b) TMV@ZIF is Subjected to Denaturing Conditions Such as Heat and Organic Solvents; (c) Stressed TMV@ZIF is Exfoliated with EDTA; (d) Recovered TMV Surface Integrity is Characterized by ELISA
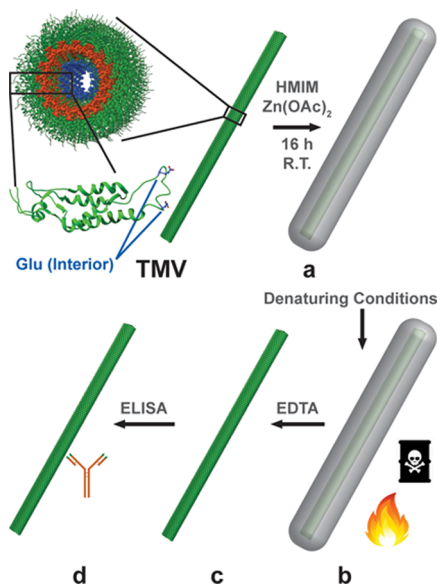
both interior and exterior surfaces independently, has given TMV a unique appeal beyond vaccine development as the structure tolerates attachment of dyes,[53] sensors,[54,55] contrast agents,[56] and bioactive molecules.[57,58] The multivalent nature of TMV comes from its 2130 identical coat proteins arranged helically around a 4 nm central pore where the viral RNA is located. This allows many bioconjugations to the same virus particle, increasing local concentration of active sites and immobilizing them, which is one reason it is thought to be such a useful platform for vaccine development.[50−52]

Because TMV is an established preclinical vaccine platform, it is a reasonable model to test the efficacy of thermal protection when encapsulated inside ZIF-8. While it is possible to remove the ZIF-8 shell to obtain pristine TMV, we wondered if this additional step was unnecessary. Indeed, it

had occurred to us that the dissolution of ZIF-8, which happens slowly in biological media, may present a method to formulate "slow release" agents for proteins—an area of active research interest.[59,60] We thus sought to determine if we could simply leave the TMV inside the protective ZIF-8 shell and inject this composite subcutaneously in a mouse model as a method to slowly release TMV, producing an immune response similar to injecting native TMV subcutaneously.

We can quantify changes to the surfaces of TMV as a result of ZIF-8 growth and removal using anti-TMV antibodies measured in an enzyme-linked immunosorbent assay (ELISA). A damaged or unfolded protein at the virus surface will not interact strongly with their complementary antibodies and this loss of affinity will manifest as a diminished ELISA response. The TMV@ZIF composite was subjected to stressors, including heat and denaturing solvents, the ZIF shell was removed, and the recovered protein was examined by ELISA to confirm surface intactness. Tobacco plant infection and in vivo studies further demonstrate the viability of ZIF-8 as a protective shell. Finally, we conducted longitudinal in vivo studies to ascertain the toxicity and immunogenicity of the TMV@ZIF-8 when implanted subcutaneously. Our results show that this strategy has considerable potential to operate concurrently as a substrate to stabilize proteins at above ambient conditions as well as deliver them effectively intact and in a more linear dose.

■ RESULTS AND DISCUSSION

TMV@ZIF can be prepared in a number of different morphologies[17] ranging from bulky rhombic dodecahedra containing hundreds of viruses to discrete rod-shaped core−shell bionanoparticles with a shell thickness tunable from 10 to 40 nm. Each of these morphologies have different colloidal and dispersion characteristics and for this study the following criteria were considered: (i) the composite made had to be dispersible in solution for easy in vivo injection, and (ii) the kinetics of shell dissolution should allow for complete dissolution of all in vivo administered ZIF-8 by the end of our 1-month study. When we attempted to suspend rhombic dodecahedra, they settled out of solution too quickly and clogged the syringe. This is in line with literature reports that particles larger than 1000 nm tend to settle rather quickly, making them a difficult material for injection.[61,62] We chose to continue forward with rods, as the ∼350 nm particle size allow for them to be easily dispersed into solution and the shell exfoliates more rapidly than the larger rhombic dodecahedra. We thus set out to determine whether the ZIF-8 shell would increase the stability of TMV and if it could be delivered in vivo. The encapsulation of TMV into ZIF-8 crystals was obtained by mixing TMV (0.111 mg) with an aqueous solution of 2-methylimidazole (400 mM, 3.0 mL), followed by an aqueous solution of zinc acetate (20 mM, 1.5 mL) (Scheme 1). After 16 h, the TMV@ZIF particles were collected by centrifugation at 4300g and the shell diameter and rodlike morphology were verified by scanning electron microscopy (SEM) (Figure 1a). The morphology of TMV@ZIF is clearly different from the common rhombic dodecahedral native ZIF-8 crystals.

TMV@ZIF was then stressed under various conditions to determine the stability of the encapsulated virus surface. Stability versus various solvents was tested: soaking in methanol, ethyl acetate, and 6 M guanidinium chloride—a common protein denaturant[63]—overnight. Thermal stability
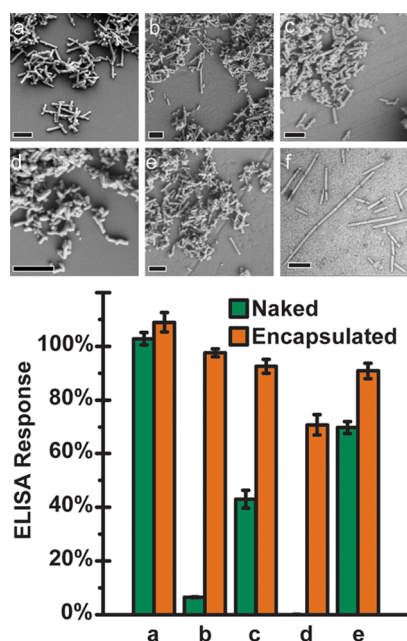
Figure 1. Top: SEM images of TMV@ZIF (a) non-stressed, (b) heating at 100 °C for 20 min, and after soaking overnight in (c) methanol, (d) 6 M guanidinium chloride, and (e) ethyl acetate. Scale bars represent 1 μm. (f) TEM image of exfoliated nonstressed TMV. Scale bar is 200 nm. Bottom: The ELISA response of naked and encapsulated TMV subject to no stress (a), heating (b), methanol (c), 6 M guanidinium chloride (d), and ethyl acetate (e). These labels correlate to the SEM images a−e above. The percentages range from buffer blank (0% TMV) to a separate internal control of nonstressed naked TMV (100% TMV).

was tested by heating TMV@ZIF to 100 °C for 20 min. After stressing, samples retained their rodlike morphology, as seen in SEM (Figure 1b−e). The poststressed composites were exfoliated in EDTA, desalted, and resuspended in 0.1 M sodium phosphate buffer. The protein concentrations were then determined by the Lowry assay, and all samples were diluted to 5.0×10^{-4} mg/mL and the ELISA response was determined. Because changes in the viral protein surface were being investigated, the ELISA results were normalized to naked nonstressed TMV (100%) and buffer blank (0%) for comparison between the two. We were pleased to discover that the process of the shell formation and exfoliation did not significantly alter the protein surface and that the shell confers considerable protection to TMV when exposed to high temperatures. For instance, the percent difference between naked TMV and TMV@ZIF when heated to 100 °C for 20 min was 165.0% (Figure 1 bottom, Table S1). Likewise, the percent difference between protected and unprotected exposure to the strongly denaturing guanidinium chloride was 199.2% (Figure 1 bottom). We were also able to demonstrate that the ZIF was able to confer protection against other denaturing organic solvents (Table S1).

We then set out to determine whether encapsulating TMV would damage the RNA. To assess the protection that TMV@ZIF has on the RNA of TMV, *Nicotiana benthamiana* plants were inoculated with phosphate buffer as a negative control and TMV@ZIF, TMV@ZIF exfoliated with EDTA, and native TMV as a positive control. The infection of *N. benthamiana* depends on the disassembly of the capsid to liberate the intact

viral RNA and begin replication. Consequently, any damage to the RNA will reduce viral load in plants.

Inoculated leaves were collected after 10 days post infection. Visually, the control plants remained green and the other plants withered (Figure 2a−d). ELISA was performed on 1 g
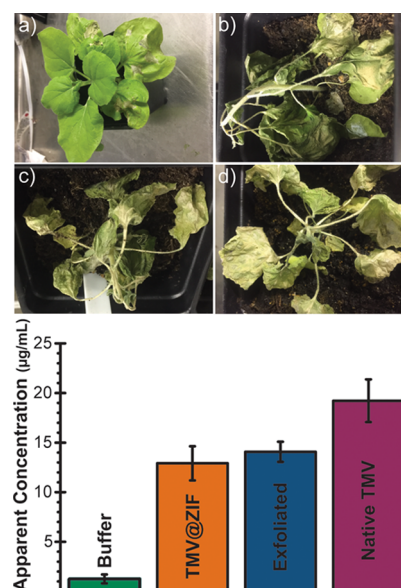

Figure 2. Top: *N. benthamiana* plants 10 days after inoculation with (a) 0.1 M pH 7.4 potassium phosphate buffer as a negative control, (b) TMV@ZIF, (c) exfoliated TMV@ZIF, and (d) native TMV as a positive control. Bottom: A bar graph showing the viral recovery of TMV from 1 g of harvested leaves measured by ELISA. Leaves were inoculated with buffer as a negative control, TMV@ZIF, exfoliated TMV@ZIF, and native TMV as a positive control.

of leaves macerated in 10 mL of extraction buffer and centrifuged to remove the large plant matter. Because the relative amount of TMV present in the leaf matter was being investigated, the ELISA results were fit to a standard curve of native TMV and the results are reported as apparent TMV concentration in μg/mL. The TMV@ZIF, exfoliated TMV@ZIF, and native TMV plants showed a clear increase in ELISA response compared to the buffer-inoculated plants, with percent differences of 164.32% (a 10-fold increase), 167.01% (an 11-fold increase), and 175.29% (a 15-fold increase), respectively (Figure 2 bottom). This indicates that the TMV remains virulent and that the RNA survives the encapsulation and exfoliation process.

We next turned our attention to in vivo studies on murine models to determine (i) whether the virus would release from the protective ZIF shell in vivo, (ii) how the anti-TMV IgG production against subcutaneously administered TMV@ZIF compares to native TMV, and (iii) the biocompatibility of the TMV@ZIF composite. In order to determine relative antibody production and optimize serum dilutions, two groups ($n = 4$) of BALB/c test mice were either noninjected or injected subcutaneously with native TMV and blood drawn after 10 days. In the test mice, there was a clear anti-TMV ELISA response in mice injected with native TMV compared to noninjected mice after 10 days, and an optimal serum dilution range of 200× to 5000× was found (Figure S5). To continue our investigation, 12 BALB/c mice were divided into three groups ($n = 4$) and subcutaneously injected on day 0, 2, 4, and 6 with saline, native TMV, or TMV@ZIF. Multiple injections
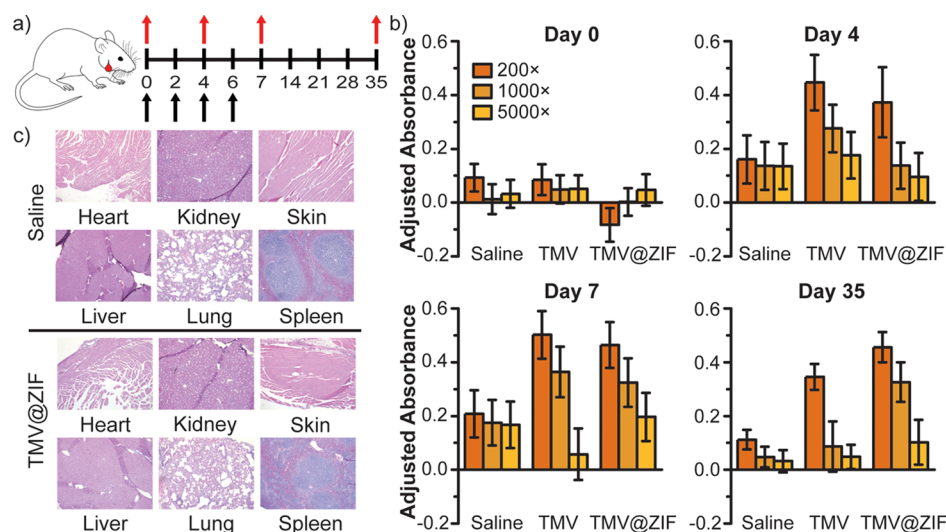
Figure 3. (a) Time schedule showing the days the mice were injected (black arrows) and submandibular blood withdrawals were performed (red arrows). Serum samples were diluted 200×, 1000×, and 5000×. (b) ELISA response for each time point, buffer blank subtracted. (c) Hematoxylin & eosin Y (H&E) staining of saline- and TMV@ZIF-injected mice.

were administered to enhance the antibody production levels in mice. We hypothesized that the TMV@ZIF would protect the encapsulated TMV in the body for as long as native TMV and result in a similar antibody production level. Submandibular blood draws were conducted on day 0, 4, 7, and 35 (Figure 3a). The ELISA response, which measures the production of mouse antibodies against TMV, shows that the TMV@ZIF elicits an antibody response comparable to naked TMV (Figure 3b). Antibody production typically depends upon successful uptake by antigen-presenting cells (APCs)—for instance macrophages and dendritic cells—in the body. This means that the shell is being removed before or during APC uptake. Exactly what is happening requires further study; however, there is literature precedent[35] that ZIF-8 can dissolve in the presence of cell media and it is not unexpected that ZIF-8 would dissociate in the interstitial fluids of the subcutaneous region prior to cellular uptake. The antibody levels that were detected for the composites were comparable to that of naked TMV, confirming that the TMV@ZIF does not need to be exfoliated before administration. 5 days after the last blood withdrawal, H&E-stained images were taken on various organs for each mouse to further evaluate TMV@ZIF biocompatibility. No visual difference could be determined between mice injected with saline and with TMV@ZIF (Figure 3c). This confirms the biocompatibility of TMV@ZIF, following multiple subcutaneous injections with no apparent toxicity or behavioral changes in the mice. Although some literature has shown in vitro toxicity,[35,64] our study has concluded that these results may not translate in vivo.

Our method depends upon the slow degradation of ZIF-8 in vivo by physiological salts and macromolecules, suggesting that encapsulation and protein−ZIF composite formation may be an intriguing way to prolong a linear dose of protein-based drugs. This could be especially useful for the administration of insulin and vaccines, which typically require multiple injections over time to achieve a sustained effect.[65] Histology of the tissue at the subcutaneous site of administration at the conclusion of the study—which consisted of four consecutive TMV@ZIF injections—did not uncover any residual material, tissue damage, or scarring, which lead us to suspect that the full

dose was being absorbed into the animal, as shown in Figure 3c. To better understand the rate at which TMV@ZIF was taken up by the mouse, we conducted time-dependent in vivo imaging using TMV labeled on its interior with the red-emitting fluorophore Cy5 (Cy5-TMV, λ_{ex} = 647 nm, λ_{em} = 666 nm, Figure S2). This labeled TMV was encapsulated inside ZIF-8, which caused a quenching of the red fluorescence. This fluorescence of Cy5-TMV was restored in full when the shell was removed, providing a clear indication of shell removal (Figure S6). For this study, 6 BALB/c mice were divided into two groups (n = 3), shaved to remove the hair on their torso and limbs, and injected subcutaneously with either unencapsulated Cy5-TMV or Cy5-TMV@ZIF and imaged over two weeks. The images shown in Figure 4b show that, prior to injection, the only fluorescence comes from the hairs near the head. As shown in the series of images in Figure 4c, subcutaneous injection of Cy5-TMV decayed slowly over a period of 120 h. In contrast, the Cy5-TMV@ZIF fluoresced weakly at first, followed by an increase and then gradual decay. After 288 h, the fluorescence at the injection site for the encapsulated material returned to the baseline.

■ CONCLUSIONS

The results of this study strongly indicate that ZIF-8 coatings not only provide protection against denaturing solvents and heat, but the nucleation and growth of the crystalline lattice does not alter the secondary or tertiary structure of protein and protein ensembles. Further, the shell does not significantly damage the viral RNA. The ZIF-8 shells are exceptionally easy to synthesize on proteins, their composites are formed in a few seconds, and are ready to use within hours. It is clear from histology data that prolonged exposure to ZIF-8 does not alter the tissue morphology at either the injection site or distal organs. Qualitatively, we saw no behavior changes in mice following administration, nor did any mice become ill or die as a result of prolonged exposure to TMV@ZIF composites. On the other hand, in vivo data clearly suggest that the administration of equal quantities of immunogenic protein yielded identical antibody responses, showing that the release of the protein from the ZIF shell occurs to completion. This
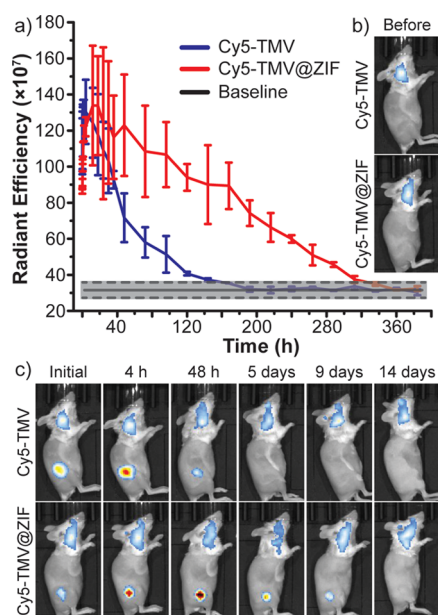
Figure 4. (a) Fluorescence intensity over time. The baseline is the average fluorescence intensity of four mice before injection. The dashed line represents the error of the baseline. (b) Images of the mice prior to injection of Cy5-TMV or Cy5-TMV@ZIF. The mice were shaved and the only initial fluorescence comes from the hairs on the head. (c) After injection and time point images of Cy5-TMV or Cy5-TMV@ZIF.

was further corroborated with time-dependent in vivo imaging studies, which showed a time-delayed release of the injection over the course of 14 days—a property of ZIF-8 we aim to exploit in subsequent studies. Taken together, these data strongly suggest that ZIF-8-based shells may provide a method to concurrently protect and deliver proteinaceous drugs safely.

■ EXPERIMENTAL METHODS

Preparation of TMV@ZIF. A 0.111 mg of TMV was briefly mixed with 3 mL of 400 mM 2-methylimidazole and to this solution was rapidly added 1.5 mL of 20 mM zinc acetate and the solution was swirled for 20 s. Flocculates appeared within a few seconds. The solution was left on the bench at R.T. for 16−18 h, then centrifuged at 4300g for 20 min and the supernatant was discarded. The pellet was washed twice with ultrapure water and used as is.

TMV@ZIF Stressing. Three batches of TMV@ZIF were combined and either left as is (nonstressed), soaked in 1 mL of methanol, ethyl acetate, or 6 M guanidinium chloride overnight, or heated to 100 °C in a water bath for 20 min. Naked TMV samples were stressed in the same manner, with 0.333 mg of TMV soaked in 1 mL solvent overnight, or heated to 100 °C for 20 min. Encapsulated samples were collected via centrifugation at 4300g for 20 min, rinsed with ultrapure water, and exfoliated in EDTA overnight. Exfoliated and naked samples were buffer exchanged into 0.1 M pH 7.4 sodium phosphate buffer in a centrifugal filter for concentration determination by the Lowry assay and then diluted to 5×10^{-4} mg/mL for ELISA measurements.

Plant Inoculation. *N. benthamiana* plants were divided into four groups ($n = 6$) and inoculated with either 0.1 M pH 7.4 potassium phosphate buffer (negative control), naked TMV in potassium phosphate buffer (positive control), TMV@ZIF in ultrapure water, or exfoliated TMV@ZIF in potassium phosphate buffer. Solutions were prepared such that 50 μL of solution delivered 5 μg of TMV, and 50 μL per leaf was used. Plants were collected after 10 d, macerated in buffer, soaked overnight, and centrifuged to remove large plant matter. The apparent TMV concentrations of the supernatants were determined by ELISA.

In Vivo Antibody Response. BALB/c mice were divided into three groups ($n = 4$), and subcutaneously injected with 200 μL of saline, naked TMV in saline, or TMV@ZIF in saline. TMV solutions were prepared such that 200 μL delivered 10 μg of TMV. Injections were administered on days 0, 2, 4, and 6, and submandibular blood draws were taken on days 0, 4, 7, and 35. Blood was centrifuged to remove erythrocytes and the resulting serum anti-TMV IgG levels were determined by ELISA. At the conclusion of the study, the mice were sacrificed, and histological analysis was performed.

In Vivo Fluorescence Imaging. BALB/c mice were fed a nonfluorescent diet and shaved to remove autofluorescence, divided into three groups and injected with 200 μL of saline ($n = 4$), Cy5-TMV ($n = 3$), or Cy5-TMV@ZIF ($n = 3$). The TMV-containing solutions were prepared such that 200 μL delivered 10 μg of TMV. In vivo fluorescence images were taken at a series of timepoints until the fluorescence levels of the Cy5-injected mice returned to the baseline levels of the saline-injected mice.

■ ASSOCIATED CONTENT

ⓢ Supporting Information

The Supporting Information is available free of charge on the ACS Publications website at DOI: 10.1021/acsami.8b20504.

> Further experimental details, materials, instrumentation, TMV isolation protocol, synthetic procedures, ^{1}H NMR spectra, excitation and emission spectra, UV−vis absorbance, PXRD spectra, ELISA response, regions of interest and their radiant efficiencies, and ELISA values (PDF)

■ AUTHOR INFORMATION

Corresponding Author
*E-mail: Gassensmith@utdallas.edu.

ORCID ⓞ
Michael A. Luzuriaga: 0000-0001-6128-8800
Raymond P. Welch: 0000-0003-3114-8801
Madushani Dharmarwardana: 0000-0002-3086-047X
Candace E. Benjamin: 0000-0002-9211-718X
Shaobo Li: 0000-0002-4178-0897
Jeremiah J. Gassensmith: 0000-0001-6400-8106

Author Contributions
§M.A.L. and R.P.W. contributed equally to this manuscript. Primary manuscript writing and editing was done by M.A.L., R.P.W., and J.J.G. Mouse injections and blood draws were performed by M.A.L. ELISA, TEM, PXRD, and Cy5 quantification were performed by R.P.W. Synthesis of TMV@ZIF and SEM were performed by R.P.W. and M.A.L. Synthesis and bioconjugation of Cy5 was performed by M.D. Histology was performed by M.A.L. and C.E.B. NMR was performed by A.S. Mouse handling and biodistribution was performed by M.A.L. and S.P. TMV infection, purification, and characterization was performed by M.A.L., R.P.W., S.L., L.H.T., and C.T.C. Funding was raised by J.J.G.

Notes
The authors declare no competing financial interest.

■ REFERENCES

(1) Leader, B.; Baca, Q. J.; Golan, D. E. Protein Therapeutics: A Summary and Pharmacological Classification. *Nat. Rev. Drug Discovery* **2008**, *7*, 21−39.

(2) Chen, Z.; Li, N.; Li, S.; Dharmarwardana, M.; Schlimme, A.; Gassensmith, J. J. Viral Chemistry: The Chemical Functionalization of Viral Architectures to Create New Technology. *Wiley Interdiscip. Rev.: Nanomed. Nanobiotechnol.* **2016**, *8*, 512−534.

(3) Thirumalai, D.; Reddy, G. Are Native Proteins Metastable? *Nat. Chem.* **2011**, *3*, 910−911.

(4) Mallamace, F.; Corsaro, C.; Mallamace, D.; Vasi, S.; Vasi, C.; Baglioni, P.; Buldyrev, S. V.; Chen, S.-H.; Stanley, H. E. Energy Landscape in Protein Folding and Unfolding. *Proc. Natl. Acad. Sci. U.S.A.* **2016**, *113*, 3159−3163.

(5) Carmichael, S. P.; Shell, M. S. Entropic (De) Stabilization of Surface-Bound Peptides Conjugated with Polymers. *J. Chem. Phys.* **2015**, *143*, 243103.

(6) Pisal, S.; Wawde, G.; Salvankar, S.; Lade, S.; Kadam, S. Vacuum Foam Drying for Preservation of LaSota Virus: Effect of Additives. *AAPS PharmSciTech* **2006**, *7*, E30−E37.

(7) LeClair, D. A.; Cranston, E. D.; Lichty, B. D.; Xing, Z.; Thompson, M. R. Consecutive Spray Drying to Produce Coated Dry Powder Vaccines Suitable for Oral Administration. *ACS Biomater. Sci. Eng.* **2018**, *4*, 1669−1678.

(8) Sridhar, B. V.; Janczy, J. R.; Hatlevik, Ø.; Wolfson, G.; Anseth, K. S.; Tibbitt, M. W. Thermal Stabilization of Biologics with Photoresponsive Hydrogels. *Biomacromolecules* **2018**, *19*, 740−747.

(9) Welch, R. P.; Lee, H.; Luzuriaga, M. A.; Brohlin, O. R.; Gassensmith, J. J. Protein−Polymer Delivery: Chemistry from the Cold Chain to the Clinic. *Bioconjugate Chem.* **2018**, *29*, 2867−2883.

(10) Lee, P. W.; Shukla, S.; Wallat, J. D.; Danda, C.; Steinmetz, N. F.; Maia, J.; Pokorski, J. K. Biodegradable Viral Nanoparticle/Polymer Implants Prepared via Melt-Processing. *ACS Nano* **2017**, *11*, 8777−8789.

(11) Liu, Y.; Lee, J.; Mansfield, K. M.; Ko, J. H.; Sallam, S.; Wesdemiotis, C.; Maynard, H. D. Trehalose Glycopolymer Enhances Both Solution Stability and Pharmacokinetics of a Therapeutic Protein. *Bioconjugate Chem.* **2017**, *28*, 836−845.

(12) Vrdoljak, A.; Allen, E. A.; Ferrara, F.; Temperton, N. J.; Crean, A. M.; Moore, A. C. Induction of Broad Immunity by Thermostabilised Vaccines Incorporated in Dissolvable Microneedles Using Novel Fabrication Methods. *J. Controlled Release* **2016**, *225*, 192−204.

(13) Doonan, C.; Riccò, R.; Liang, K.; Bradshaw, D.; Falcaro, P. Metal−Organic Frameworks at the Biointerface: Synthetic Strategies and Applications. *Acc. Chem. Res.* **2017**, *50*, 1423−1432.

(14) Alsaiari, S. K.; Patil, S.; Alyami, M.; Alamoudi, K. O.; Aleisa, F. A.; Merzaban, J. S.; Li, M.; Khashab, N. M. Endosomal Escape and Delivery of CRISPR/Cas9 Genome Editing Machinery Enabled by Nanoscale Zeolitic Imidazolate Framework. *J. Am. Chem. Soc.* **2018**, *140*, 143−146.

(15) Liang, K.; Ricco, R.; Doherty, C. M.; Styles, M. J.; Bell, S.; Kirby, N.; Mudie, S.; Haylock, D.; Hill, A. J.; Doonan, C. J.; Falcaro, P. Biomimetic Mineralization of Metal-Organic Frameworks as Protective Coatings for Biomacromolecules. *Nat. Commun.* **2015**, *6*, 7240.

(16) Li, S.; Dharmarwardana, M.; Welch, R. P.; Ren, Y.; Thompson, C. M.; Smaldone, R. A.; Gassensmith, J. J. Template-Directed Synthesis of Porous and Protective Core−Shell Bionanoparticles. *Angew. Chem., Int. Ed.* **2016**, *55*, 10691−10696.

(17) Li, S.; Dharmarwardana, M.; Welch, R. P.; Benjamin, C. E.; Shamir, A. M.; Nielsen, S. O.; Gassensmith, J. J. Investigation of Controlled Growth of Metal−Organic Frameworks on Anisotropic Virus Particles. *ACS Appl. Mater. Interfaces* **2018**, *10*, 18161−18169.

(18) Wang, C.; Luan, J.; Tadepalli, S.; Liu, K.-K.; Morrissey, J. J.; Kharasch, E. D.; Naik, R. R.; Singamaneni, S. Silk-Encapsulated Plasmonic Biochips with Enhanced Thermal Stability. *ACS Appl. Mater. Interfaces* **2016**, *8*, 26493−26500.

(19) Rosi, N. L.; Eddaoudi, M.; Kim, J.; O'Keeffe, M.; Yaghi, O. M. Advances in the Chemistry of Metal-Organic Frameworks. *CrystEngComm* **2002**, *4*, 401−404.

(20) McGuire, C. V.; Forgan, R. S. The Surface Chemistry of Metal−Organic Frameworks. *Chem. Commun.* **2015**, *51*, 5199−5217.

(21) Banerjee, R.; Phan, A.; Wang, B.; Knobler, C.; Furukawa, H.; O'keeffe, M.; Yaghi, O. M. High-Throughput Synthesis of Zeolitic Imidazolate Frameworks and Application to CO_2 Capture. *Science* **2008**, *319*, 939−943.

(22) Hayashi, H.; Côté, A. P.; Furukawa, H.; O'Keeffe, M.; Yaghi, O. M. Zeolite A Imidazolate Frameworks. *Nat. Mater.* **2007**, *6*, 501−506.

(23) Li, L.; Yang, L.; Wang, J.; Zhang, Z.; Yang, Q.; Yang, Y.; Ren, Q.; Bao, Z. Highly Efficient Separation of Methane from Nitrogen on a Squarate-Based Metal-Organic Framework. *AIChE J.* **2018**, *64*, 3681−3689.

(24) Huxley, M. T.; Burgun, A.; Ghodrati, H.; Coghlan, C. J.; Lemieux, A.; Champness, N. R.; Huang, D. M.; Doonan, C. J.; Sumby, C. J. Protecting-Group-Free Site-Selective Reactions in a Metal−Organic Framework Reaction Vessel. *J. Am. Chem. Soc.* **2018**, *140*, 6416−6425.

(25) Otake, K.-i.; Cui, Y.; Buru, C. T.; Li, Z.; Hupp, J. T.; Farha, O. K. Single-Atom-Based Vanadium Oxide Catalysts Supported on Metal−Organic Frameworks: Selective Alcohol Oxidation and Structure−Activity Relationship. *J. Am. Chem. Soc.* **2018**, *140*, 8652−8656.

(26) Fan, C.; Lv, X.; Liu, F.; Feng, L.; Liu, M.; Cai, Y.; Liu, H.; Wang, J.; Yang, Y.; Wang, H. Silver Nanoclusters Encapsulated into Metal−Organic Frameworks with Enhanced Fluorescence and Specific Ion Accumulation toward the Microdot Array-Based Fluorimetric Analysis of Copper in Blood. *ACS Sens.* **2018**, *3*, 441−450.

(27) Zhuang, J.; Kuo, C.-H.; Chou, L.-Y.; Liu, D.-Y.; Weerapana, E.; Tsung, C.-K. Optimized Metal−Organic-Framework Nanospheres for Drug Delivery: Evaluation of Small-Molecule Encapsulation. *ACS Nano* **2014**, *8*, 2812−2819.

(28) Adhikari, C.; Das, A.; Chakraborty, A. Zeolitic Imidazole Framework (ZIF) Nanospheres for Easy Encapsulation and Controlled Release of an Anticancer Drug Doxorubicin Under Different External Stimuli: A Way Toward Smart Drug Delivery System. *Mol. Pharmaceutics* **2015**, *12*, 3158−3166.

(29) Zheng, H.; Zhang, Y.; Liu, L.; Wan, W.; Guo, P.; Nyström, A. M.; Zou, X. One-Pot Synthesis of Metal−Organic Frameworks with Encapsulated Target Molecules and Their Applications for Controlled Drug Delivery. *J. Am. Chem. Soc.* **2016**, *138*, 962−968.

(30) Lázaro, I. A.; Haddad, S.; Rodrigo-Muñoz, J. M.; Marshall, R. J.; Sastre, B.; del Pozo, V.; Fairen-Jimenez, D.; Forgan, R. S. Surface-Functionalization of Zr-Fumarate MOF for Selective Cytotoxicity and Immune System Compatibility in Nanoscale Drug Delivery. *ACS Appl. Mater. Interfaces* **2018**, *10*, 31146−31157.

(31) Majewski, M. B.; Howarth, A. J.; Li, P.; Wasielewski, M. R.; Hupp, J. T.; Farha, O. K. Enzyme Encapsulation in Metal−Organic Frameworks for Applications in Catalysis. *CrystEngComm* **2017**, *19*, 4082−4091.

(32) Riccò, R.; Liang, W.; Li, S.; Gassensmith, J. J.; Caruso, F.; Doonan, C.; Falcaro, P. Metal−Organic Frameworks for Cell and Virus Biology: A Perspective. *ACS Nano* **2018**, *12*, 13−23.

(33) Nadar, S. S.; Rathod, V. K. Encapsulation of Lipase Within Metal-Organic Framework (MOF) with Enhanced Activity Intensified Under Ultrasound. *Enzyme Microb. Technol.* **2018**, *108*, 11−20.

(34) Li, P.; Moon, S.-Y.; Guelta, M. A.; Harvey, S. P.; Hupp, J. T.; Farha, O. K. Encapsulation of a Nerve Agent Detoxifying Enzyme by a Mesoporous Zirconium Metal−Organic Framework Engenders

Thermal and Long-Term Stability. *J. Am. Chem. Soc.* **2016**, *138*, 8052−8055.

(35) Hoop, M.; Walde, C. F.; Riccò, R.; Mushtaq, F.; Terzopoulou, A.; Chen, X.-Z.; demello, A. J.; Doonan, C. J.; Falcaro, P.; Nelson, B. J.; Puigmartí-Luis, J.; Pané, S. Biocompatibility Characteristics of the Metal Organic Framework ZIF-8 for Therapeutical Applications. *Appl. Mater. Today* **2018**, *11*, 13−21.

(36) Maddigan, N. K.; Tarzia, A.; Huang, D. M.; Sumby, C. J.; Bell, S. G.; Falcaro, P.; Doonan, C. J. Protein Surface Functionalisation as a General Strategy for Facilitating Biomimetic Mineralisation of ZIF-8. *Chem. Sci.* **2018**, *9*, 4217−4223.

(37) Liao, F.-S.; Lo, W.-S.; Hsu, Y.-S.; Wu, C.-C.; Wang, S.-C.; Shieh, F.-K.; Morabito, J. V.; Chou, L.-Y.; Wu, K. C.-W.; Tsung, C.-K. Shielding Against Unfolding by Embedding Enzymes in Metal−Organic Frameworks via a de Novo Approach. *J. Am. Chem. Soc.* **2017**, *139*, 6530−6533.

(38) Wang, C.; Sun, H.; Luan, J.; Jiang, Q.; Tadepalli, S.; Morrissey, J. J.; Kharasch, E. D.; Singamaneni, S. Metal−Organic Framework Encapsulation for Biospecimen Preservation. *Chem. Mater.* **2018**, *30*, 1291−1300.

(39) Wang, C.; Sudlow, G.; Wang, Z.; Cao, S.; Jiang, Q.; Neiner, A.; Morrissey, J. J.; Kharasch, E. D.; Achilefu, S.; Singamaneni, S. Metal-Organic Framework Encapsulation Preserves the Bioactivity of Protein Therapeutics. *Adv. Healthcare Mater.* **2018**, *7*, 1800950.

(40) Zhu, Q.; Zhuang, W.; Chen, Y.; Wang, Z.; Villacorta Hernandez, B.; Wu, J.; Yang, P.; Liu, D.; Zhu, C.; Ying, H.; Zhu, Z. Nano-Biocatalysts of Cyt c@ZIF−8/GO Composites with High Recyclability via a de Novo Approach. *ACS Appl. Mater. Interfaces* **2018**, *10*, 16066−16076.

(41) Deng, H.; Grunder, S.; Cordova, K. E.; Valente, C.; Furukawa, H.; Hmadeh, M.; Gandara, F.; Whalley, A. C.; Liu, Z.; Asahina, S.; Kazumori, H.; O'Keeffe, M.; Terasaki, O.; Stoddart, J. F.; Yaghi, O. M. Large-Pore Apertures in a Series of Metal-Organic Frameworks. *Science* **2012**, *336*, 1018−1023.

(42) Chen, Y.; Li, P.; Modica, J. A.; Drout, R. J.; Farha, O. K. Acid-Resistant Mesoporous Metal−Organic Framework Toward Oral Insulin Delivery: Protein Encapsulation, Protection, and Release. *J. Am. Chem. Soc.* **2018**, *140*, 5678−5681.

(43) Li, P.; Modica, J. A.; Howarth, A. J.; Vargas L, E.; Moghadam, P. Z.; Snurr, R. Q.; Mrksich, M.; Hupp, J. T.; Farha, O. K. Toward Design Rules for Enzyme Immobilization in Hierarchical Mesoporous Metal-Organic Frameworks. *Chem* **2016**, *1*, 154−169.

(44) Zhang, Y.; Wang, F.; Ju, E.; Liu, Z.; Chen, Z.; Ren, J.; Qu, X. Metal-Organic-Framework-Based Vaccine Platforms for Enhanced Systemic Immune and Memory Response. *Adv. Funct. Mater.* **2016**, *26*, 6454−6461.

(45) Lyu, F.; Zhang, Y.; Zare, R. N.; Ge, J.; Liu, Z. One-Pot Synthesis of Protein-Embedded Metal−Organic Frameworks with Enhanced Biological Activities. *Nano Lett.* **2014**, *14*, 5761−5765.

(46) Xu, A.-W.; Ma, Y.; Cölfen, H. Biomimetic Mineralization. *J. Mater. Chem.* **2007**, *17*, 415−449.

(47) Xu, M.; Zhu, J.; Wang, F.; Xiong, Y.; Wu, Y.; Wang, Q.; Weng, J.; Zhang, Z.; Chen, W.; Liu, S. Improved In Vitro and In Vivo Biocompatibility of Graphene Oxide Through Surface Modification: Poly(Acrylic Acid)-Functionalization is Superior to PEGylation. *ACS Nano* **2016**, *10*, 3267−3281.

(48) Maurer, P.; Jennings, G. T.; Willers, J.; Rohner, F.; Lindman, Y.; Roubicek, K.; Renner, W. A.; Müller, P.; Bachmann, M. F. A Therapeutic Vaccine for Nicotine Dependence: Preclinical Efficacy, and Phase I Safety and Immunogenicity. *Eur. J. Immunol.* **2005**, *35*, 2031−2040.

(49) Stephanopoulos, N.; Francis, M. B. Choosing an Effective Protein Bioconjugation Strategy. *Nat. Chem. Biol.* **2011**, *7*, 876−884.

(50) Rybicki, E. P. Plant-Based Vaccines Against Viruses. *Virol. J.* **2014**, *11*, 205.

(51) Banik, S.; Mansour, A. A.; Suresh, R. V.; Wykoff-Clary, S.; Malik, M.; McCormick, A. A.; Bakshi, C. S. Development of a Multivalent Subunit Vaccine Against Tularemia Using Tobacco Mosaic Virus (TMV) Based Delivery System. *PLoS One* **2015**, *10*, e0130858.

(52) Gasanova, T. V.; Petukhova, N. V.; Ivanov, P. A. Chimeric Particles of Tobacco Mosaic Virus as a Platform for the Development of Next-Generation Nanovaccines. *Nanotechnol. Russ.* **2016**, *11*, 227−236.

(53) Masarapu, H.; Patel, B. K.; Chariou, P. L.; Hu, H.; Gulati, N. M.; Carpenter, B. L.; Ghiladi, R. A.; Shukla, S.; Steinmetz, N. F. Physalis Mottle Virus-Like Particles as Nanocarriers for Imaging Reagents and Drugs. *Biomacromolecules* **2017**, *18*, 4141−4153.

(54) Dharmarwardana, M.; Martins, A. F.; Chen, Z.; Palacios, P. M.; Nowak, C. M.; Welch, R. P.; Li, S.; Luzuriaga, M. A.; Bleris, L.; Pierce, B. S.; Sherry, A. D.; Gassensmith, J. J. Nitroxyl Modified Tobacco Mosaic Virus as a Metal-Free High-Relaxivity MRI and EPR Active Superoxide Sensor. *Mol. Pharmaceutics* **2018**, *15*, 2973−2983.

(55) Bäcker, M.; Koch, C.; Eiben, S.; Geiger, F.; Eber, F.; Gliemann, H.; Poghossian, A.; Wege, C.; Schöning, M. J. Tobacco Mosaic Virus as Enzyme Nanocarrier for Electrochemical Biosensors. *Sens. Actuators, B* **2017**, *238*, 716−722.

(56) Anderson, C. E.; Donnola, S. B.; Jiang, Y.; Batesole, J.; Darrah, R.; Drumm, M. L.; Brady-Kalnay, S. M.; Steinmetz, N. F.; Yu, X.; Griswold, M. A.; Flask, C. A. Dual Contrast-Magnetic Resonance Fingerprinting (DC-MRF): A Platform for Simultaneous Quantification of Multiple MRI Contrast Agents. *Sci. Rep.* **2017**, *7*, 8431.

(57) Pitek, A. S.; Wang, Y.; Gulati, S.; Gao, H.; Stewart, P. L.; Simon, D. I.; Steinmetz, N. F. Elongated Plant Virus-Based Nanoparticles for Enhanced Delivery of Thrombolytic Therapies. *Mol. Pharmaceutics* **2017**, *14*, 3815−3823.

(58) Finbloom, J. A.; Han, K.; Aanei, I. L.; Hartman, E. C.; Finley, D. T.; Dedeo, M. T.; Fishman, M.; Downing, K. H.; Francis, M. B. Stable Disk Assemblies of a Tobacco Mosaic Virus Mutant as Nanoscale Scaffolds for Applications in Drug Delivery. *Bioconjugate Chem.* **2016**, *27*, 2480−2485.

(59) Cossé, A.; König, C.; Lamprecht, A.; Wagner, K. G. Hot Melt Extrusion for Sustained Protein Release: Matrix Erosion and In Vitro Release of PLGA-Based Implants. *AAPS PharmSciTech* **2017**, *18*, 15−26.

(60) Ren, Y.; Shi, X.; Sun, Q.; Sun, L. Dual-Controlled Oral Colon-Targeted Delivery of Bovine Insulin Based on Mesoporous Phosphonate. *Mater. Res. Bull.* **2013**, *48*, 4850−4855.

(61) Majewski, M. B.; Noh, H.; Islamoglu, T.; Farha, O. K. NanoMOFs: Little Crystallites for Substantial Applications. *J. Mater. Chem. A* **2018**, *6*, 7338−7350.

(62) Chen, T.-T.; Yi, J.-T.; Zhao, Y.-Y.; Chu, X. Biomineralized Metal-Organic Framework Nanoparticles Enable Intracellular Delivery and Endo-Lysosomal Release of Native Active Proteins. *J. Am. Chem. Soc.* **2018**, *140*, 9912−9920.

(63) Jha, S. K.; Marqusee, S. Kinetic Evidence for a Two-Stage Mechanism of Protein Denaturation by Guanidinium Chloride. *Proc. Natl. Acad. Sci. U.S.A.* **2014**, *111*, 4856−4861.

(64) Zhang, H.; Chen, W.; Gong, K.; Chen, J. Nanoscale Zeolitic Imidazolate Framework-8 as Efficient Vehicles for Enhanced Delivery of CpG Oligodeoxynucleotides. *ACS Appl. Mater. Interfaces* **2017**, *9*, 31519−31525.

(65) Schade, D. S. The Timing of Meal Insulin Administration. *Endocr. Pract.* **2017**, *23*, 1482−1484.